Journal of Molecular and Cellular Cardiology Plus 11 (2025) 100273

Contents lists available at ScienceDirect

Journal of Molecular and Cellular Cardiology Plus

journal homepage: www.journals.elsevier.com/journal-of-molecular-andcellular-cardiology-plus

An optimized plasmalogen modulating dietary supplement provides greater protection in a male than female mouse model of dilated cardiomyopathy

Teleah G. Belkin [a,b,c], Emma I. Masterman [a], Gunes S. Yildiz [a], Helen Kiriazis [a,e], Natalie A. Mellett [a], Jonathon Cross [a], Kyah Grigolon [a], Akshima Dogra [a], Daniel Donner [a,e], Roger Chooi [a], Amy Liang [a], Andrew R. Kompa [b], Junichi Sadoshima [d], Amanda J. Edgley [b], David W. Greening [a,c,e,i], Peter J. Meikle [a,f,g], Yow Keat Tham [a,e,f,g,*,1], Julie R. McMullen [a,e,g,h,i,j,**,1]

[a] Baker Heart and Diabetes Institute, Melbourne, VIC, Australia
[b] Department of Medicine, The University of Melbourne, VIC, Australia
[c] School of Translational Medicine, Monash University, Melbourne, VIC, Australia
[d] Department of Cell Biology and Molecular Medicine, Rutgers New Jersey Medical School, Newark, NJ, USA
[e] Baker Department of Cardiometabolic Health, The University of Melbourne, VIC, Australia
[f] Department of Diabetes, School of Translational Medicine, Monash University, Clayton, VIC, Australia
[g] Baker Department of Cardiovascular Research, Translation and Implementation, La Trobe University, Bundoora, VIC, Australia
[h] Department of Physiology, Monash University, VIC, Australia
[i] Monash Alfred Baker Centre for Cardiovascular Research, Faculty of Medicine Nursing and Health Sciences, Monash University, VIC, Australia
[j] Heart Research Institute, Newtown, NSW, Australia

ARTICLE INFO

Keywords:
Alkylglycerols (AG)
Dilated cardiomyopathy (DCM)
Lipidomics
Heart failure
Plasmalogens

ABSTRACT

We previously reported that plasmalogens, a class of phospholipids, were decreased in a setting of dilated cardiomyopathy (DCM). Plasmalogen levels can be modulated via a dietary supplement called alkylglycerols (AG) which has demonstrated benefits in some disease settings. However, its therapeutic potential in DCM remained unknown. To determine whether an optimized AG supplement could restore plasmalogen levels and attenuate cardiac dysfunction/pathology, we placed a cardiac-specific transgenic DCM mouse model of both sexes on chow +/−1.5 % AG supplementation at ~10 weeks of age for 16 weeks. Cardiac function was assessed by echocardiography, tissues were collected for histological and molecular analyses including lipidomics and proteomics via liquid chromatography-mass spectrometry. AG supplementation increased total plasmalogens in DCM hearts and attenuated lung congestion of both sexes, but only prevented cardiac dysfunction in males. This was associated with attenuated cardiac and renal enlargement, a more favorable pro-cardiac gene expression profile, and a trend for lower cardiac fibrosis. By lipidomics, specific d18:1 ceramide species associated with cardiac pathology were lower in the DCM hearts from mice on the AG diet, and tetralinoleoyl cardiolipins, a lipid crucial for mitochondrial function was restored with AG supplementation. Proteomic analysis of hearts from male DCM mice receiving AG supplementation revealed enrichment in mitochondrial protein network, as well as upregulation of extracellular matrix binding proteins including agrin, a protein associated with cardiac regeneration. In summary, AG supplementation restored plasmalogens in DCM hearts but showed greater therapeutic potential in males than females.

1. Introduction

Pathological cardiac remodeling occurs in response to a chronic cardiac stress or genetic mutations and can be associated with inflammation, fibrosis, autophagy, and cellular dysfunction involving oxidative stress, metabolic and signaling pathway impairments,

* Correspondence to: Y.K. Tham, Metabolomics Laboratory, Baker Heart and Diabetes Institute, 75 Commercial Road, Melbourne, VIC 3004, Australia.
** Correspondence to: J.R. McMullen, Heart Research Institute, 7 Eliza Street, Newton, NSW 2042, Australia.
E-mail addresses: yowkeat.tham@baker.edu.au (Y.K. Tham), julie.mcmullen@hri.org.au (J.R. McMullen).
[1] Co-senior authors.

https://doi.org/10.1016/j.jmccpl.2024.100273
Received 21 November 2024; Accepted 1 December 2024
Available online 4 December 2024

mitochondrial dysfunction, and left ventricular enlargement. This is often a precursor for the development and progression of heart failure (HF) [1]. Recent developments in the field of lipidomics have allowed for a more in-depth characterization of the lipidome in experimental models of pathological remodeling and HF. As cardiac myocytes change shape during pathological remodeling, there is significant remodeling of the cardiac myocyte membranes including lipids within the membranes [3]. Lipid metabolism is an intricate physiological process essential for maintaining homeostasis, hormone control, and nutrient regulation [4]. Lipids are essential biomolecules that play a significant role in providing structural support for cell membranes but also have diverse cellular functions such as energy storage and signaling [5]. However, when the composition of lipid species becomes disrupted within an organelle or the cell itself, lipid metabolism dysfunction can occur. This can result in serious lipid-related diseases such as obesity, type 2 diabetes, and cardiovascular disease (CVD) [6]. A subclass of phospholipids, known as plasmalogens, are highly abundant in the heart, brain, and skeletal muscle, making up >15 % of total phospholipids [1,2]. Previous studies have shown that plasmalogens can be beneficial in settings of pathology including CVD and diabetes [9]. However, the therapeutic potential for the failing heart was unclear.

In a previous study undertaken in our laboratory, we showed that plasmalogens were decreased in the heart of a mouse model with dilated cardiomyopathy (DCM). Alkylglycerols (AGs) represent lipid intermediates that have the ability to modulate plasmalogen subspecies via supplementation in the diet. Thus, to restore a major plasmalogen species in the heart (p18:0), we previously used a dietary AG called batyl alcohol (BA). The DCM mouse model presents with cardiac dysfunction, left ventricular enlargement, pulmonary edema, and cardiac fibrosis [10]. When administered BA for a period of 16 weeks, the DCM mouse model showed a significant increase in p18:0 plasmalogen levels compared to the chow mice. However, there was no significant attenuation of cardiac pathology or dysfunction. Upon further lipidomic analysis, an unanticipated feedback loop associated with BA supplementation revealed a concurrent decrease in p16:0 and p18:1 plasmalogen subspecies compared to chow fed DCM mice [11]. The decrease in these other plasmalogens may explain why we observed no cardiac protection. The main goals of the current study were to examine whether an optimized AG supplementation comprising of batyl alcohol (BA, p18:0), selachyl alcohol (SA, p18:1), and chimyl alcohol (CA, p16:0) could, 1) restore p18:0, p18:1, and p16:0 plasmalogen levels in a mouse model of DCM and, 2) attenuate/reverse cardiac pathology and markers of HF.

2. Methods

2.1. Experimental animals

The Alfred Health and Education Precinct Animal Ethics Committee granted approval for the care and experimental use of mice. The Alfred Medical Research and Education Precinct Animal Centre housed mice in a temperature controlled, 12-hour light-dark cycle environment (6 am–6 pm). Mice were euthanized at the end of the study with 300-400 mg/kg of sodium pentobarbital intraperitoneally. Tissues and plasma were collected for histological, molecular, lipidomic, and proteomic analyses.

2.2. Tg mouse model with dilated cardiomyopathy (DCM)

The transgenic (Tg) mouse model develops DCM due to the overexpression of mammalian sterile 20-like kinase 1 (Mst1). The expression of the transgene in cardiomyocytes is driven by the α-myosin heavy chain (αMHC) promoter, resulting in specific expression in Tg mice shortly after birth [3]. The DCM phenotype is distinguished by dilation of the atria and ventricles, accompanied by wall thinning of the left ventricle, interstitial fibrosis, pulmonary edema, and severe systolic ventricular dysfunction [3]. Endogenous Mst1 is known to be increased or activated in both patients with dilated cardiomyopathy and mouse models of myocardial infarction [4,5]. While no mouse model will completely replicate what occurs in humans, it has features consistent with human DCM including thinning of the ventricular walls, apoptosis, fibrosis and activation of p38. Tg and non-transgenic (Ntg) mice were generated by crossing heterozygous Tg mice with Ntg mice.

2.3. BA, SA, and CA dietary supplementation

BA, SA, and CA supplemented, and chow diets were produced by Speciality Feeds (WA, Australia). The diet contained 1.5 % BA, SA, and CA per 100 g of chow.

2.4. Echocardiography-assessment of cardiac function and dimensions

Echocardiography (echo) was performed using the Vevo 2100 Fujifilm Visual Sonics Ultrasound machine with a MS 550D probe on anaesthetized mice (1.8 % isoflurane) to assess the longitudinal changes in heart size and function. Systolic function was assessed by parasternal long-axis (pLAX) B-mode.

2.5. Lipidomic analyses

Ventricles were homogenized in 120 μL PBS using the Branson digital probe-sonicator. Homogenates underwent a 1:20 dilution and protein concentration (absorbance of 562 nm) was determined by using the Pierce™ BCA protein assay kit. Homogenates were diluted with 1× PBS (5 mg/mL of ventricle). 10 μL of internal standard was added to each sample. 200 μL of Chloroform: Methanol (ChCl3/MeOH) was added, and samples were placed in the bath sonicator (room temperature (RT), 30 min). Samples were spun in the Beckman Coulter Microfuge 18 centrifuge (16,060*g*, 10 min). ~200 μL of supernatant was transferred to a 0.5 mL polypropylene 96-well plate and samples were dried using the Speedivac and pump (one hour and a half). Extracted lipid samples were reconstituted with 50 μL of water saturated butanol and sonicated (10 min). 50 μL of MeOH with Ammonium Formate was added to each sample and centrifuged in the Heraeus multifuge 1S-R (4,000*g*, 5 min). 100 μL of sample was aliquoted into glass vials. Lipidomic analyses of lipid extracts were performed by liquid chromatography using the Agilent 1290 liquid chromatography system combined with the Agilent 6495 triple quadruple mass spectrometer as previously described [6].

2.6. RNA extraction

Ventricles were homogenized in 500 μL Trizol reagent and incubated (RT, 5 min). Samples were centrifuged (4 °C, 10 min, 18,720 g). The supernatant was transferred to new 1.5 mL tubes and 0.1 mL of chloroform was added. Samples were vortexed and incubated on ice. Samples were centrifuged (4 °C, 15 min, 18,720 g) and the aqueous phase was transferred into new 1.5 mL tubes. 0.5 mL of isopropanol was added and samples were incubated at −20 °C overnight. The supernatant was removed and 1 mL of 75 % Diethyl pyrocarbonate (DEPC) treated ethanol (EtOH) was added. Samples were spun (4 °C, 2 min, 21,380 g). The supernatant was removed and an additional 1 mL of 75 % DEPC EtOH was added. Samples were centrifuged (4 °C, 5 min, 21,380 g) and the supernatant was removed. Samples were air dried, and the pellet was resuspended in 50 μL Nuclease Free water (NF-H_2O) and stored at −80 °C.

2.7. Synthesis of cDNA and the assessment of gene expression via real time-quantitative PCR

25 ng/μL of complementary DNA (cDNA) was generated from extracted RNA from ventricles. 20 μL aliquots were added to the 96-well plate and placed in the Applied Biosystems Veriti Thermal Cycler for

PCR using the pre-programmed cycling conditions: cDNA High Capacity. Expression was normalized against Hypoxanthine phosphoribosyl transferase 1 (Hprt1).

2.8. Masson's trichrome staining for fibrosis quantification

Ntg and DCM ventricles were processed and embedded in paraffin wax. Ventricular tissues were sectioned (4 μm) and placed on Superfrost Plus Adhesion microscope slides. Slides were placed in the oven (60 °C, 10 min) for deparaffinization. Slides were then placed in histolene (5 min, ×2), 100 % ethanol (3 min, ×2) and then 70 % ethanol (3 min). Slides were then introduced into dH_2O and transferred into Weigert's Iron Haematoxylin (5 min) to stain nuclei black. Slides were stained with Biebrichscarlet-Acid Fuchsin (5 min) before being rinsed in dH_2O (3 min). By agitating the slides, the sections were washed in Phosphotungstic acid solution (10 min) and then placed in Aniline Blue (10 min). Slides were rinsed in dH_2O, dehydrated in 95 % ethanol and 100 % ethanol, and cleared in histolene (5 min, ×2) before being coverslipped. Fibrosis was quantified using Aperio ImageScope [v12.4.6.5003] software. The area of fibrosis/collagen was expressed relative to area of the LV.

2.9. Proteomics

2.9.1. Proteomic sample preparation

Ventricles from female and male mice (Ntg chow, Ntg diet, DCM chow, DCM diet (n = 4 per group)) were lysed on ice in lysis buffer (8 M urea in 50 mM HEPES pH 8.0 with Halt™ Protease/Phosphatase Inhibitor Cocktail (#78442, Thermo Fisher Scientific) and extracted by pulse tip-probe sonication on ice and quantified by microBCA (#23235, Thermo Fisher Scientific) as previously described [6]. All samples were normalized (10 μg) then subjected to reduction and alkylation, followed by solid-phase interaction proteomic sample preparation, as previously described [7]. Briefly, protein samples were mixed with Sera-Mag Speed Beads (GE LifeScience) at a 10:1 beads-to-protein ratio, with protein-bound-beads reconstituted and exposed to trypsin (V5113, Promega) and Lys-C (121-05063, FUJIFILM Wako Pure Chemical Corporation) at 1:50 and 1:100 enzyme-to-substrate ratio respectively, followed by overnight digestion at 37 °C with shaking. Peptide digests were collected from the supernatant and acidified with formic acid to a final 2 % (v/v) concentration before vacuum lyophilization and reconstitution in 0.07 % (v/v) trifluoroacetic acid in MS-grade water.

2.9.2. LC-MS/MS

Spectra were acquired in data independent acquisition on an Q Exactive HF-X benchtop Orbitrap mass spectrometer coupled to an UltiMate™ NCS-3500RS nano-HPLC (Thermo Fisher Scientific) as previously described [6]. Full scan MS were performed in the *m/z* range of 350 to 1100 with a 60,000 resolution, using an automatic gain control (AGC) of 3 × 10 [6], maximum injection time of 50 ms and 1 microscan. MS2 was set to 15,000 resolution, 1e6 AGC target and the first fixed mass set to 120 *m/z*. Default charge state set to 2 and recorded in centroid mode. For optimized acquisition, we performed a total of 38 scan windows with staggered 20 *m/z* isolation window applied with 28 % normalized collision energy as described [65]. Data were acquired using Xcalibur software v4.5 (Thermo Fisher Scientific).

2.9.3. Data processing and analysis

Identification and quantification of peptides and proteins was performed using DIA-NN neural network and interference correction (v1.8) with mass spectra searched against *Mus musculus* (mouse) reference proteome (55,398) supplemented with common contaminants as previously described [6]. Spectral libraries were predicted using the deep learning algorithm employed in DIA-NN with Trypsin/P, allowing up to 1 missed cleavage as described [6,8]. The precursor change range was set to 1–4, and the *m/z* precursor range was set to 300–1800 for peptides consisting of 7–30 amino acids with N-term methionine excision and cysteine carbamidomethylation enabled as a fixed modification with 0 maximum number of variable modifications. The mass spectra were analyzed using default settings with a false discovery rate (FDR) of 1 % for precursor identifications and match between runs (MBR) enabled for replicates. Venn diagrams were created using www.interactivenn.net. Perseus (v2.0.7.0) was applied for downstream data processing and analysis. Stringent data quality inclusion was applied with 70 % protein group quantification for proteins within each group. Protein intensities were $\log_2$ transformed and normalized using quantile normalization. Hierarchical clustering was performed in Perseus using Euclidean distance and average linkage clustering. Proteins were subjected to Principle Component Analysis (PCA) with missing values imputed from normal distribution (width 0.3, downshift 1.8) and unpaired student's *t*-test. g:Profiler database were utilized for Gene Ontology functional enrichment and network/pathway analysis, significance $p < 0.05$. Multi-parameter (non-parametric) differential expression analysis (ANOVA, $p < 0.05$) was performed in Perseus, with increased (positive) and decreased (negative) expression profiles (FC) for individual proteins relative to chow groups baseline (average, $\log_2$ intensity values). All proteomics data and analyses are provided in a Supplementary Data Set (labelled Supplementary Tables 5–30 within the results).

2.10. Statistical analyses

Results are presented as mean ± SEM. Two-way ANOVA followed by Tukey's post-hoc test was used unless stated otherwise. Lipidomic datasets were assessed via R Studio (4.3.1) using two-way ANOVA followed by Šidák's multiple comparisons test and *t*-test comparisons. Graphs were produced using GraphPad Prism 9.3.0 (GraphPad Software, Inc). $p < 0.05$ was considered statistically significant.

3. Results

Male and female Ntg and DCM mice (~10-weeks-old) were fed a diet consisting of chow or AG supplementation comprised of BA, SA + CA for 16 weeks (Fig. 1A). Dietary supplementation with the AG (BA, SA + CA) lipid intermediates in mice bypasses the rate limiting step of plasmalogen biosynthesis within the peroxisome, allowing for increased production of ether lipids, including ones with phosphatidylethanolamine (PE) and phosphatidylcholine (PC) head groups: [PE(O), PC(O), PE(P) and PC(P)] (Fig. 1B). As we previously reported [9], plasmalogen levels were lower in the ventricles and plasma of the DCM model vs. Ntg (Fig. 1C). In this study, the goal was to restore plasmalogen levels in the DCM model and examine whether this had a favorable impact on cardiac function and remodeling.

3.1. Restoration and increased plasmalogen levels via AG supplementation in male DCM mice attenuated pathological features associated with DCM and heart failure

PCA was conducted on the lipidome of male ventricles and plasma to analyze the distribution of lipids between genotypes (Ntg and DCM) and diets (chow and AG diet) (Fig. 1D). PCA plots demonstrate a clear separation between AG supplemented and chow fed cohorts for both the ventricular and plasma lipidome, in addition to separation between the diseased DCM vs. Ntg lipidomes. Given that the AG diet consists of the BA, SA, and CA lipid intermediates that target the ether lipids with 18:0, 18:1, and 16:0 fatty alcohol chains, we sought to evaluate changes to the aforementioned plasmalogen species [PC(P), PE(P)] and their precursors [PC(O), PE(O)]. Total plasmalogen precursors: PC(O) and PE(O)-(O16:0, O18:0, and O18:1) were significantly increased in the ventricles and plasma of the AG supplemented male Ntg and DCM mice vs. controls (Fig. 1E & F). This was also true for the majority of the plasmalogen subspecies (Fig. 1E & F).

Heart size and heart weight normalized to tibia length (HW/TL) ratio

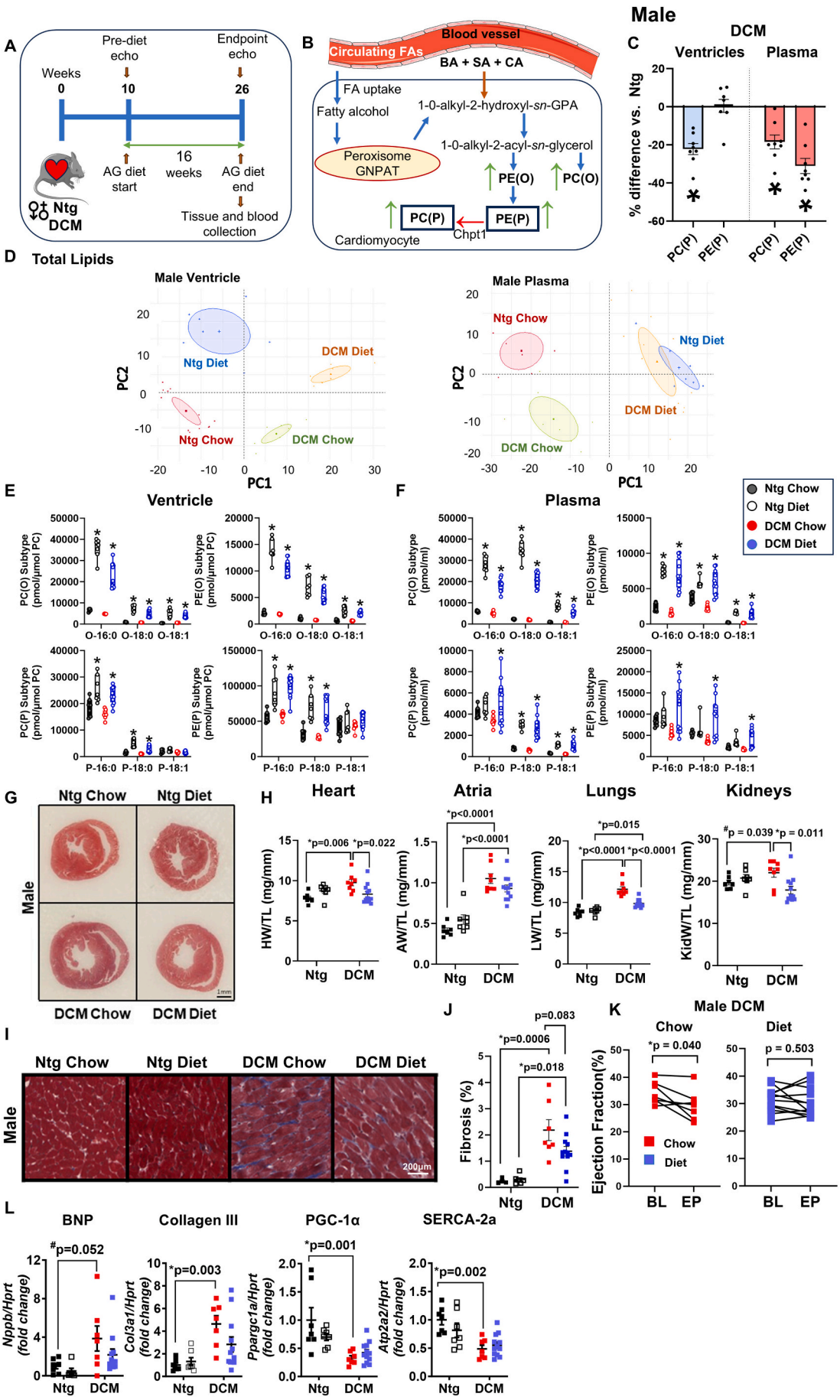

(caption on next page)

Fig. 1. AG supplementation attenuates cardiac pathology in male DCM hearts. A) Experimental timeline over the 16-weeks of chow or AG supplementation. B) BA + SA + CA used as lipid intermediates to enter the plasmalogen biosynthesis pathway. C) Scatter bar graphs showing phosphatidylcholine (PC) and phosphatidylethanolamine (PE) plasmalogens in male DCM hearts and plasma as a % vs. Ntg mice. Ntg chow = 7, DCM chow = 8. *p < 0.05. D) PCA plots of total lipids in hearts and plasma of male Ntg and DCM mice given chow or AG supplementation. E) Boxplots showing total plasmalogens and total plasmalogen precursors in ventricles in male Ntg and DCM chow fed or AG supplemented mice. Data analyzed using two-way ANOVA followed by Šidák's multiple comparison's test. Ntg chow = 7, Ntg diet = 7, DCM chow = 8, DCM diet = 12. *p < 0.05. F) Boxplots showing total plasmalogens and total plasmalogen precursors in plasma in male Ntg and DCM chow fed or AG supplemented mice. Data analyzed using two-way ANOVA followed by Šidák's multiple comparison's test. Ntg chow = 7, Ntg diet = 7, DCM chow = 8, DCM diet = 12. *p < 0.05. G) Representative heart images of male Ntg and DCM chow or AG supplemented mice. H) Scatterplots showing male heart weight/tibia length (HW/TL), atria weight/tibia length (AW/TL), lung weight/tibia length (LW/TL), kidney weight/tibia length (KidW/TL) of Ntg and DCM mice fed chow or AG supplementation. Data evaluated by two-way ANOVA followed by Tukey's post-hoc analysis test. Ntg chow = 7, Ntg diet = 7, DCM chow = 8, DCM diet = 12. *p < 0.05. I) Representative images of male Ntg and DCM chow or AG supplemented mouse ventricle tissue stained with Masson's Trichrome. J) Scatterplot showing Masson's Trichrome staining of ventricle tissue of male Ntg and DCM chow or AG supplemented mice. Data evaluated by two-way ANOVA followed by Tukey's post-hoc analysis test. Ntg chow = 4, Ntg diet = 6, DCM chow = 7, DCM diet = 12. *p < 0.05. K) Pairwise graphs showing ejection fraction of chow and AG supplemented male DCM mice from baseline to endpoint. Data analysed by paired *t*-test. DCM chow = 8, DCM diet = 12. *p < 0.05. L) Scatterplots showing qPCR analysis of cardiac, fibrotic, and metabolic markers. B-type natriuretic peptide/Hypoxanthine-guanine phosphoribosyl transferase (Nppb/Hrpt), Collagen III (Col3a1/Hrpt), Peroxisome proliferator-activated receptor gamma co-activator 1-alpha (PGC-1α/Hrpt), Sarcoplasmic/endoplasmic reticulum Ca^2-ATPase 2a (Atp2a2/Hrpt) of male Ntg and DCM mice fed chow or AG supplementation. Data analyzed by two-way ANOVA followed by Tukey's post-hoc analysis. Ntg chow = 7, Ntg diet = 7, DCM chow = 8, DCM diet = 12. *p < 0.05.

of male DCM chow mice was greater than male Ntg chow mice (Fig. 1G & H). When supplemented with the AG diet, HW/TL of male DCM mice was significantly lower than DCM chow mice, and not significantly different from Ntg mice (Fig. 1G & H, Supp Table 1; AG diet had no significant effect in Ntg mice). Atria weight normalized to tibia length (AW/TL) ratio was significantly increased in the DCM model vs. Ntg, and the AG diet had no impact on this parameter (Fig. 1H). Lung weight normalized to tibia length (LW/TL) was assessed as a measure of lung congestion due to cardiac dysfunction. The LW/TL ratio was significantly increased in the male DCM chow mice vs. Ntg chow mice, and AG supplementation in DCM mice was associated with a lower LW/TL vs. DCM chow (Fig. 1H). Kidney weight normalized to tibia length (KidW/TL) ratio was elevated in male DCM chow mice vs. Ntg chow mice (by unpaired *t*-test). KidW/TL ratio was significantly lower in male DCM mice supplemented with the AG diet vs. male DCM chow mice (Fig. 1H). There was a significant increase in cardiac fibrosis in the male DCM chow vs. Ntg mice (Fig. 1I, J), and this tended to be lower in the DCM diet mice. Cardiac function, assessed non-invasively by echocardiography before and after the intervention, demonstrated that ejection fraction (EF) was significantly decreased in the male DCM chow mice over the time course of the study i.e. between baseline and endpoint (~16 weeks) (Fig. 1K). In contrast, a significant fall in EF was not observed in the male DCM AG mice, where EF between baseline and endpoint was maintained (Fig. 1K, Supp Table 2). Raw and normalized end-diastolic LV mass over time also reflected the positive impact of the AG diet on ventricular weight in the DCM model (Supp Table 2).

Previous work has shown that cardiac stress markers such as BNP and fibrotic markers (e.g. collagen genes) are elevated in the hearts of the DCM model [9–11]. In the current study, *Nppb* (BNP) and *Col3a1* (collagen III) showed a trend or significant increase in hearts of male DCM mice vs. Ntg chow (Fig. 1L). There were no significant differences between DCM diet mice vs. Ntg diet (p > 0.1), but there were also no significant differences between the male DCM diet mice vs. DCM chow (Fig. 1L). The metabolic marker for fatty acid oxidation, *PGC-1α*, and the contractility marker, *SERCA-2a*, were significantly decreased in the hearts of DCM chow mice vs. Ntg, but not the DCM diet mice. Though, there were no significant differences between the male AG supplemented DCM mice vs. DCM chow (Fig. 1L).

3.2. AG supplementation increased plasmalogens in female DCM mice but had no effect on cardiac pathology and function

In male DCM mice, plasmalogen levels were lower in the ventricles as observed in our previous and current studies (Fig. 1C) [9]. We observed a trend for decreased PC(P) levels (p = 0.07) in the ventricles of female DCM chow, but no decrease in PE(P) levels. Similar to the males, PC(P) and PE(P) lipids were significantly lower in the plasma of female DCM vs. Ntg (Fig. 2A). PCA plots revealed distinct separation between AG supplemented and chow cohorts in conjunction with separation between the diseased DCM vs. Ntg lipidomes (Fig. 2B). Total plasmalogen precursors (O16:0, O18:0, and O18:1) were significantly increased in the ventricles and plasma of the female AG supplemented mice vs. their respective cohorts (Fig. 2C & D). The increase in plasmalogen levels following AG supplementation was also observed in the majority of plasmalogen subspecies (p16:0, p18:0, and p18:1) in the ventricles and plasma (Fig. 2C & D).

HW/TL tended to be elevated in the female DCM chow mice vs. Ntg chow but this was not significant (p = 0.068). The AG diet had no significant impact on HW/TL in the DCM mice but was not different from Ntg (Fig. 2E, Supp Table 3). AW/TL was increased in both chow and AG supplemented DCM mice vs. Ntg, with no effect of the AG supplement (Fig. 2E). LW/TL was significantly higher in the female DCM chow vs. Ntg chow, and AG supplementation was associated with a lower LW/TL ratio (Fig. 2E). KidW/TL remained unchanged across groups (Fig. 2E). Cardiac fibrosis was increased in female DCM chow mice vs. Ntg chow mice, and AG supplementation had no effect (Fig. 2F). Echocardiography demonstrated no significant changes in EF of the female DCM mice over the course of the study (~16 weeks), regardless of dietary assignments (Fig. 2G).

Nppb expression was increased in the hearts of chow and AG supplemented DCM vs. Ntg mice, with no significant differences in the DCM AG supplemented vs. chow hearts. *Col3a1* levels remained unchanged when comparing between genotype and diet cohorts (Fig. 2H). *PGC-1α* and *SERCA-2a* were decreased in the hearts of DCM chow mice vs. Ntg but AG supplementation had no effect (Fig. 2H).

3.3. AG supplementation differentially remodeled the cardiac lipidome in male and female DCM mice

Forest plots were generated to visualize changes across individual lipid species between different genotypes (Ntg and DCM) and diets (chow and AG) (Fig. 3A). The DCM cardiac lipidome compared to Ntg demonstrated key changes that occurred in the setting of HF. This included increased ceramide (Cer) levels, a lipid associated with inflammation in various settings of pathology, including cardiovascular disease [12]. Specific PE species were significantly increased, and this was also in line with a previous study that subjected mice to transverse aortic constriction [13]. Remodeling of specific cardiolipin (CL) species, reduction in ubiquinone and cardiac triacylglyceride (TG) species observed in our DCM model has also previously been demonstrated in a setting of DCM and HF [9,14]. While specific plasmalogen species were significantly increased (as noted in red; Top 10 p < 0.05 lipids), overall plasmalogen levels, in particular PC(P)s were significantly decreased.

AG supplementation in both Ntg and DCM mice were associated with

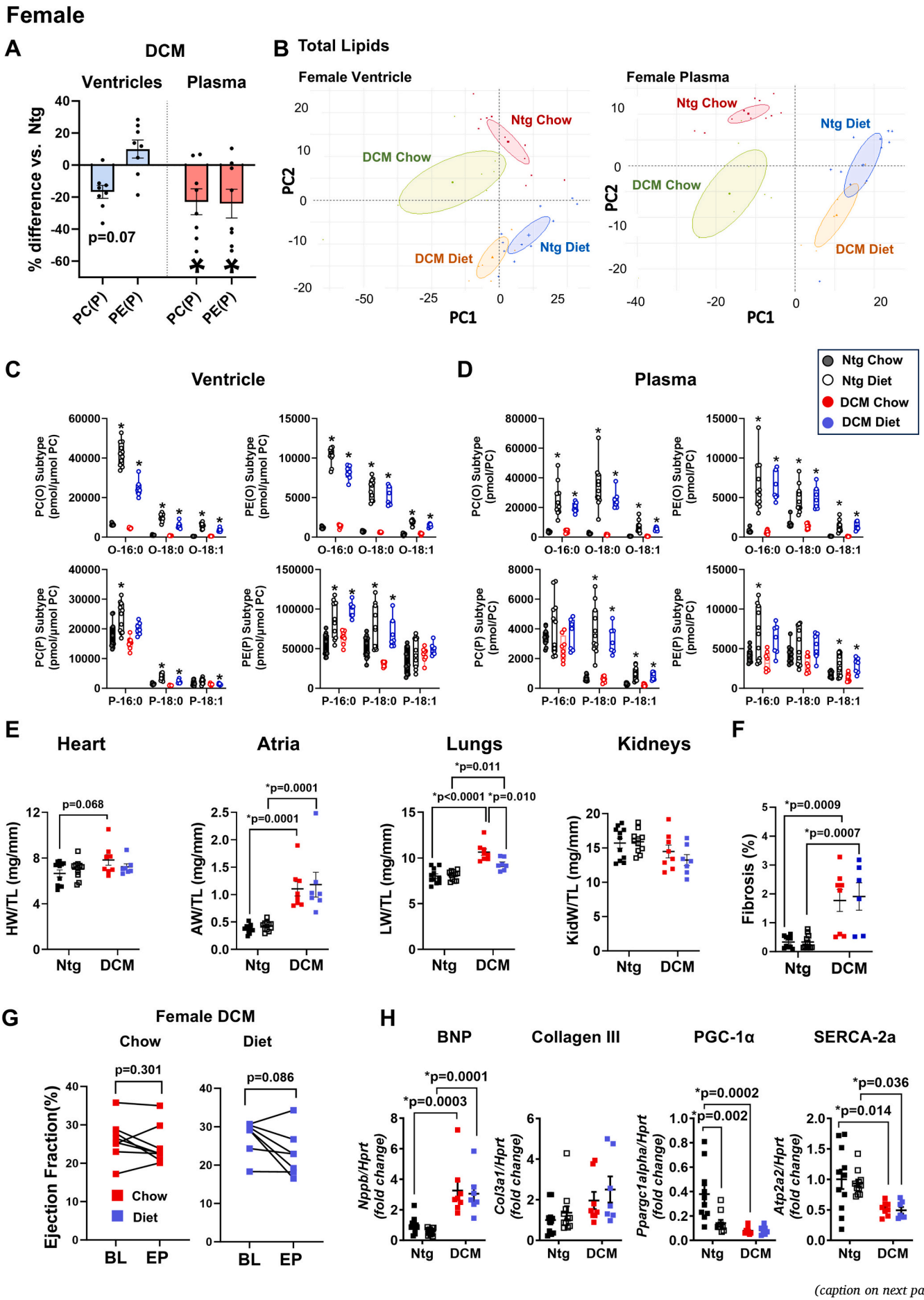

(caption on next page)

Fig. 2. AG supplementation has no effect on cardiac pathology in female DCM mice. A) Scatter bar graphs showing phosphatidylcholine (PC) and phosphatidylethanolamine (PE) plasmalogens in female DCM hearts and plasma as a % vs. Ntg mice. Ntg chow = 11, DCM chow = 8. *p < 0.05. B) PCA plots of total lipids in hearts and plasma of female Ntg and DCM mice given chow or AG supplementation. C) Boxplots showing changes in total plasmalogens and total plasmalogen precursors in ventricles in female Ntg and DCM chow fed or AG supplemented mice. Data analyzed using two-way ANOVA followed by Šidák's multiple comparison's test. Ntg chow = 11, Ntg diet = 11, DCM chow = 8, DCM diet = 7. *p < 0.05. D) Boxplots showing total plasmalogens and total plasmalogen precursors in plasma in female Ntg and DCM chow fed or AG supplemented mice. Data analyzed using two-way ANOVA followed by Šidák's multiple comparison's test. Ntg chow = 11, Ntg diet = 11, DCM chow = 8, DCM diet = 7. *p < 0.05. E) Scatterplots showing female heart weight/tibia length (HW/TL), atria weight/tibia length (AW/TL), lung weight/tibia length (LW/TL), kidney weight/tibia length (KidW/TL) of Ntg and DCM mice fed chow or AG supplementation. Data evaluated by two-way ANOVA followed by Tukey's post-hoc analysis test. Ntg chow = 11, Ntg diet = 11, DCM chow = 8, DCM diet = 7. *p < 0.05. F) Scatterplot showing Masson's Trichrome staining of ventricle tissue of female Ntg and DCM chow or AG supplemented mice. Data evaluated by two-way ANOVA followed by Tukey's post-hoc analysis test. Ntg chow = 10, Ntg diet = 11, DCM chow = 8, DCM diet = 6. *p < 0.05. G) Pairwise graphs showing ejection fraction of chow and AG supplemented female DCM mice from baseline to endpoint. Data analysed by paired *t*-test. DCM chow = 8, DCM diet = 7. H) Scatterplots showing qPCR analysis of cardiac, fibrotic, and metabolic markers. B-type natriuretic peptide/Hypoxanthine-guanine phosphoribosyl transferase (Nppb/Hrpt), Collagen III (Col3a1/Hrpt), Peroxisome proliferator-activated receptor gamma co-activator 1-alpha (PGC-1α/Hrpt), Sarcoplasmic/endoplasmic reticulum Ca^2-ATPase 2a (Atp2a2/Hrpt) of female Ntg and DCM mice fed chow or AG supplementation. Data analyzed by two-way ANOVA followed by Tukey's post-hoc analysis. Ntg chow = 11, Ntg diet = 11, DCM chow = 8, DCM diet = 7. *p < 0.05.

significant increases in plasmalogen lipids and their precursors (Figs. 1E, 3A). Consistent with previous studies, assessment of the entire cardiac lipidome also demonstrated significant increases in ether lipid species [LPC(O), LPC(P), LPE(P) and TG(O)s] [15,16]. This represents the first comprehensive report of ether lipid modulation following AG supplementation in the cardiac lipidome.

In the DCM heart, changes to the CL and Cer lipids were visualized via volcano plots to observe the changes with AG supplementation. Studies have shown that decreases in CL (72:8) [PI 36:4], also known as tetralineoylcardiolipins, result in dysfunction of mitochondrial oxidative phosphorylation [14,15]. CL (72:8) [PI 36:4] levels in DCM chow hearts were significantly reduced compared to Ntg hearts (Fig. 3B). Notably, CL (72:8) [PI 36:4] levels were associated with an increase in the DCM AG vs. DCM chow hearts (Fig. 3C). Cer, in particular Cer with a d18:1 sphingolipid backbone, has previously been linked to the development and progression of HF [16]. In the male DCM chow hearts, Cer (d18:1/16:0), Cer(d18:1/23:0), Cer(d18:1/24:0) and Cer(d18:1/24:1) were increased (Fig. 3B). Following AG supplementation, Cer(d18:1/19:0), Cer(d18:1/20:0), Cer(d18:1/21:0), Cer(d18:1/22:0), and Cer (d18:1/24:1) levels were lower (Fig. 3C).

The DCM cardiac lipidome indicates sexual dimorphism between female and male mice. The key alterations observed in male DCM hearts (increased Cer, PE and decreased TGs, ubiquinone) appeared to shift in an opposing fashion in female DCM hearts (Fig. 4A), and may partially explain the differential impact of the AG supplementation on heart function (Fig. 2G). Sex differences in cardiac metabolism are recognized [17], however, to our knowledge no comprehensive lipidomic profiling has previously been conducted on female murine HF models.

As with males, AG supplementation in female Ntg and DCM hearts were associated with significant increases in ether lipid species (Fig. 4A). In visualizing the CL species in the female DCM heart via volcano plot, it is further noted that there was no significant remodeling of CL (72:8) [PI 36:4] with AG supplementation (Fig. 4B). Additionally, there was no significant increase in total Cer levels [although two Cer species, Cer (d18:1/20:0) and Cer(d18:1/22:0) were elevated] in the female DCM heart, with no alterations observed following AG supplementation outside of a significant decrease in Cer(d18:1/20:0) and Cer(d18:1/21:0) (Fig. 4C).

3.4. Differential regulation of the proteome with AG supplementation in males and females

To further delineate potential mechanisms by which AG supplementation was associated with an attenuation of cardiac pathology in the setting of DCM, we performed proteomics on a subset of ventricular tissues from the existing cohort of mice (Fig. 5A). The PCA plot revealed a more distinct distribution of proteins between genotypes as opposed to dietary intake (Fig. 5B). Gene Ontology (GO) analyses of the DCM male heart proteome highlighted positive enrichment of specific GO terms associated with stress response, autophagic and apoptotic processes previously implicated with cardiac Mst1 overexpression [4,18] (Supp Table 5). Additionally, negative enrichment of GO terms related to the mitochondria, energy metabolism and cardiac contractility is further reflective of the DCM phenotype that develops with Mst1 overexpression [3,14] (Fig. 5C, Supp Table 6).

AG supplementation of DCM mice resulted in differential regulation of 430 proteins in the heart. Many of these upregulated proteins (AGRN, DAG1, NID1, ITGA5) were associated with GO terms that suggest significant extracellular matrix remodeling/reorganization and cell adhesion – notably, loss of or overexpression of these proteins in murine models of cardiac pathology have shown to be detrimental/protective respectively [19–21] (Fig. 5D, Supp Table 8). Furthermore, proteins associated with the mitochondrial electron transport chain/respiratory process were also enriched with AG supplementation. Negative enrichment of GO terms associated with immune response/processes may further point to less inflammation typically associated with the DCM phenotype (Supp Table 9).

Proteomic profiling of female hearts demonstrated a similar distribution to males (Fig. 5E, F). While female DCM hearts exhibited similar positive and negative enrichment of specific GO terms as the male DCM hearts (Supp Tables 12, 13), AG supplementation in female DCM hearts did not show similar positive enrichment of GO terms or the upregulation of many proteins observed in male DCM AG supplemented hearts (Fig. 5G, H). Instead, AG supplemented female DCM hearts showed positive enrichment in terms associated with proteosomes and peptidases (Supp Table 15). However, similar to AG supplemented male DCM hearts, there was also negative enrichment in GO terms related to immune responses (Supp Table 16).

4. Discussion

The therapeutic potential of enhancing plasmalogen levels in preclinical models of atherosclerosis, microglia-mediated neuroinflammation, and hepatic steatosis has previously been reported [16,22–24], but the potential of this approach in the failing heart was not clear [9,25]. In previous work undertaken in our laboratory, BA dietary supplementation was used to restore plasmalogen levels in the hearts of DCM mice. Supplementation increased a major subset of plasmalogen species (p18:0) but was not associated with improved cardiac outcomes. In-depth analyses revealed that while BA supplementation increased the p18:0 plasmalogen species, there was a concurrent reduction in the p16:0 and p18:1 subspecies; most likely due to a negative feedback mechanism within the endogenous plasmalogen biosynthesis pathway [9,26]. This unexpected feedback alteration to the cardiac plasmalogen profile of DCM BA supplemented mice may have contributed to the absence of a positive outcome [9]. Therefore, the main objective of this study was to determine whether an optimized AG dietary supplement comprised of BA, SA, and CA, could restore p18:0/

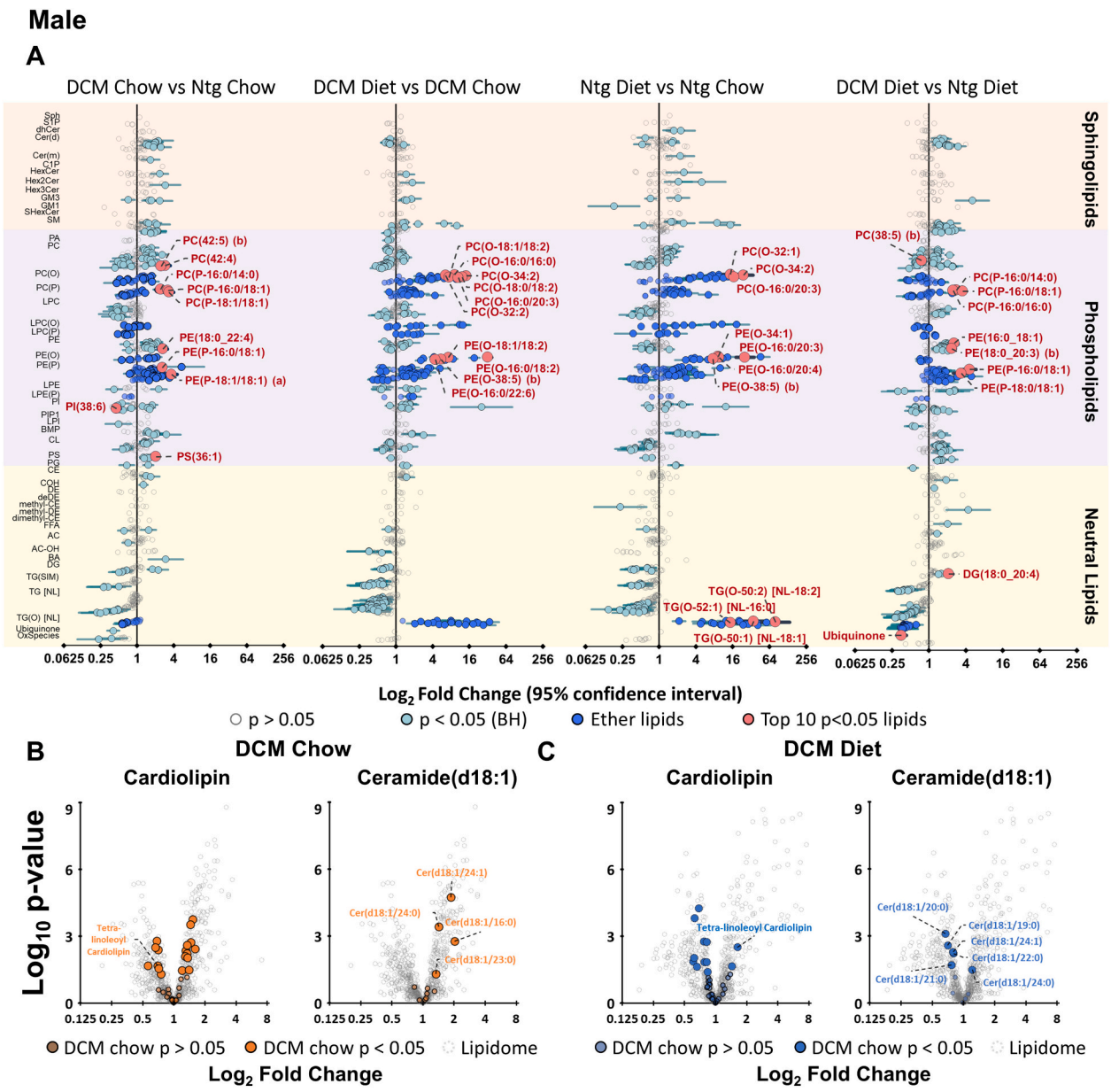

Fig. 3. AG supplementation remodels the cardiac lipidome in male DCM mice. A) Forest plots showing individual lipids in the ventricles of male Ntg and DCM mice subjected to chow or AG supplementation. Ntg chow = 7, Ntg diet = 7, DCM chow = 8, DCM diet = 12. B) Volcano plots showing changes in key lipids in the ventricles of male DCM chow mice. Left to right: Cardiolipins, Ceramides(d18:1). Solid circles highlight lipids that are significantly different. C) Volcano plots showing changes in key lipids in the ventricles of male DCM AG supplemented mice. Forest plots have each individual lipid species displayed along the y axis, grouped according to lipid class (with some across multiple lines e.g. CL), with $\log_2$(fold change) on the x axis. Left to right: Cardiolipins, Ceramides(d18:1). Solid circles highlight lipids that are significantly different.

p18:1/p16:0 plasmalogen levels in the heart and circulation of a mouse model of DCM, and subsequently restore cardiac function and attenuate cardiac pathology. The major findings of the current study were that 1) the optimized AG diet increased the majority of the plasmalogen subspecies (p18:1, p18:0, and p16:0) in Ntg and DCM mice, 2) AG supplementation protected against cardiac pathology in male but not female DCM mice, and 3) mechanistically AG supplementation in male DCM heart was associated with a cardiac proteome and lipidome reflective of sustained mitochondrial health, and less inflammation (Fig. 6).

The DCM model presents with ventricular dilatation and atrial enlargement, often with an elevation in normalized heart weight. In our prior study, BA supplementation in the DCM model did not significantly attenuate heart weight, fibrosis, or molecular markers of cardiac stress [9]. By contrast, in the present study, normalized heart size was lower in male DCM AG supplemented mice, which was associated with maintained systolic function, and a more favorable molecular cardiac phenotype. In contrast, normalized heart size remained unchanged in female DCM AG supplemented mice and the diet had no impact on systolic function or cardiac gene expression. The cardiac-specific DCM model is also associated with lung and kidney pathology and increased mass due to organ cross-talk [3,27–29]. Lung weight was elevated in both male and female DCM chow mice compared with Ntg, and the AG supplement was associated with lower normalized lung weight in both sexes. When the heart cannot pump blood effectively, this causes fluid to build up in the lungs where it impairs lung function and gas exchange, leading to hypoxia and dyspnea [30]. Previous studies have suggested that plasmalogens may play an important role in maintaining normal lung physiology [31,32]. In the current study, lung weight may be lower

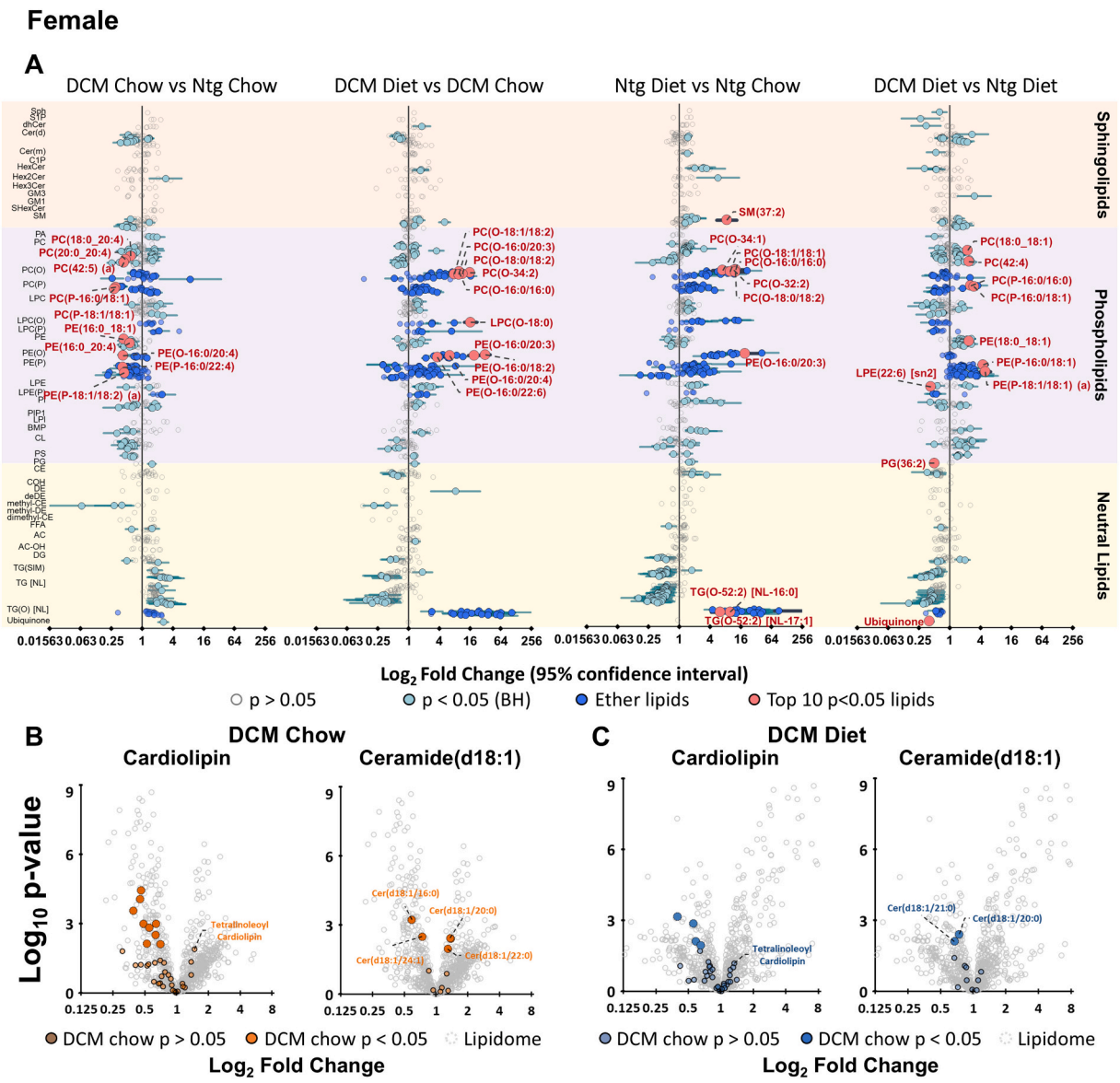

Fig. 4. The cardiac lipidome is mildly altered with AG supplementation in female DCM mice. A) Forest plots showing individual lipids in the ventricles of female Ntg and DCM mice subjected to chow or AG supplementation. Ntg chow = 11, Ntg diet = 11, DCM chow = 8, DCM diet = 7. B) Volcano plots showing changes in key lipids in the ventricles of female DCM chow mice. Left to right: Cardiolipins, Ceramides(d18:1). Solid circles highlight lipids that are significantly different. C) Volcano plots showing changes in key lipids in the ventricles of female DCM AG supplemented mice. Forest plots have each individual lipid species displayed along the y axis, grouped according to lipid class (with some across multiple lines), with $\log_2$(fold change) on the x axis. Left to right: Cardiolipins, Ceramides(d18:1). Solid circles highlight lipids that are significantly different.

in male DCM AG mice vs. DCM chow mice, in part, because cardiac function did not fall over time in DCM AG mice. An additional factor in male and female DCM AG mice, may be a direct impact of plasmalogens in the lungs. Of note, lower lung weight was also observed in our prior BA supplementation study, in which there was no impact on heart function [9].

The DCM model has previously been used as a preclinical model of cardiorenal syndrome due to defects in the kidney including renal fibrosis, inflammation, and loss of glomerular filtration rate [27–29]. Given this is a cardiac-specific Tg model, pathology or enlargement in the kidney is considered to be due to chronic dysfunction of the heart negatively affecting the kidneys [28,29,33]. In the current study, normalized kidney weight was elevated in male DCM chow mice vs. Ntg, and AG supplementation was associated with reduced kidney weight. Consistent with a non-significant increase in heart weight in female DCM chow mice, female DCM mice did not present with higher normalized kidney weights.

Mechanistically, AG supplementation is likely to have provided benefit in the male DCM model, at least in part, by the increase in plasmalogen lipid species in the heart and remodeling of the cardiac lipidome. In the male DCM model, Cer species were elevated in the heart but attenuated with AG supplementation. Elevated Cers, in particular, those with d18:1 sphingoid backbone, have been linked with the development and progression of HF [12,34,35], via the regulation of cytokine production resulting in inflammation, apoptosis and fibrosis [35–37]. Cer accumulation can also impact mitochondrial health and function, resulting in mitophagy [38]. To our knowledge, there is no evidence of AG supplementation having a direct effect on Cer levels. The lower Cer levels are probably a reflection of less cardiac pathology. Extensive phenotyping on the same DCM model used in this study demonstrated mitochondrial dysfunction and structural abnormalities [14]. The predominant CL in mitochondrial membranes [39],

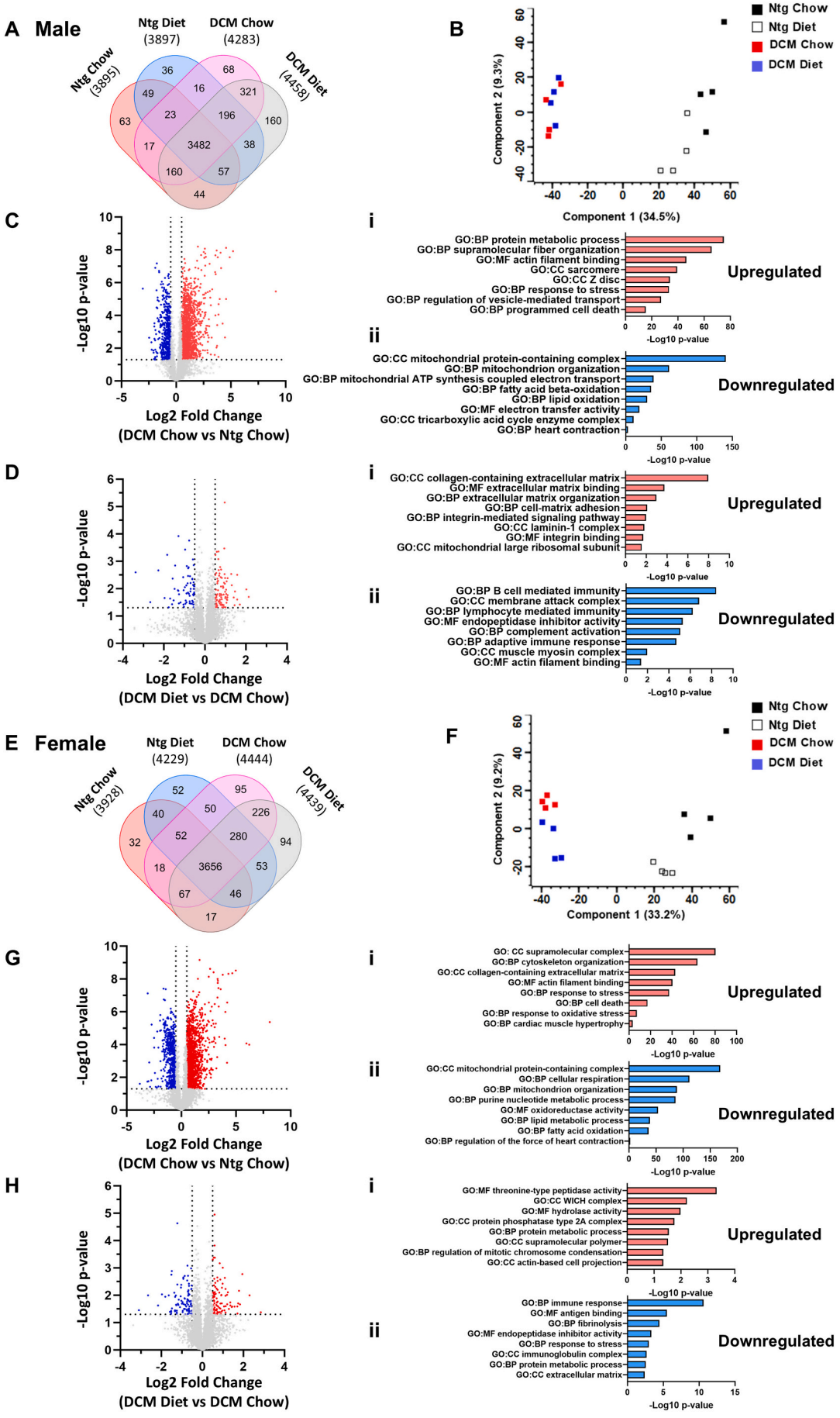

(caption on next page)

Fig. 5. AG supplementation differentially regulates the male and female proteome. A) Venn diagram of the number of proteins identified in male Ntg chow, Ntg diet, DCM chow and DCM diet mice. B) PCA plot of valid values 70 % cut off in at least one group. Based on the log_2 intensity (LFQ) transformed value of male Ntg chow, Ntg diet, DCM chow and DCM diet mice. C) Volcano plot of differential analysis of male DCM chow vs. Ntg chow Student *t*-test analysis (p-value < 0.05 ($-log_{10}$), Log_2 Fold Change <0.5 (blue) or >0.5 (red) i: Top 8 Gene Ontology enrichment of significant and unique proteins in male DCM chow using gProfiler. Term size 2–5000 $-log_{10}$ p-value. ii: Top 8 Gene Ontology enrichment of significant and unique proteins in male Ntg chow using gProfiler. Term size 2–5000 $-log_{10}$ p-value. D) Volcano plot of differential analysis of male DCM diet vs. DCM chow Student *t*-test analysis (p < 0.05 ($-log_{10}$), Log_2 Fold Change <0.5 (blue) or >0.5 (red) i: Top 8 Gene Ontology enrichment of significant and unique proteins in male DCM diet using gProfiler. Term size 2–5000 $-log_{10}$ p-value. ii: Top 8 Gene Ontology enrichment of significant and unique proteins in male DCM chow using gProfiler. Term size 2–5000 $-log_{10}$ p-value. E) Venn diagram of the number of proteins identified in female Ntg chow, Ntg diet, DCM chow and DCM diet mice. F) PCA plot of valid values 70 % cut off in at least one group. Based on the log_2 intensity (LFQ) transformed value of female Ntg chow, Ntg diet, DCM chow and DCM diet mice. G) Volcano plot of differential analysis of female DCM chow vs. Ntg chow Student *t*-test analysis (p < 0.05 ($-log_{10}$), Log_2 Fold Change < 0.5 (blue) or >0.5 (red). i: Top 8 Gene Ontology enrichment of significant and unique proteins in female DCM chow using gProfiler. Term size 2–5000 $-log_{10}$ p-value. ii: Top 8 Gene Ontology enrichment of significant and unique proteins in female Ntg chow using gProfiler. H) Volcano plot of differential analysis of female DCM diet vs. DCM chow Student *t*-test analysis (p < 0.05 ($-log_{10}$), Log_2 Fold Change < 0.5 (blue) or >0.5 (red). i: Top 8 Gene Ontology enrichment of significant and unique proteins in female DCM diet using gProfiler. Term size 2–5000. $-log_{10}$ p-value. ii: Top 8 Gene Ontology enrichment of significant and unique proteins in female DCM chow using gProfiler. Term size 2–5000 $-log_{10}$ p-value. (For interpretation of the references to colour in this figure legend, the reader is referred to the web version of this article.)

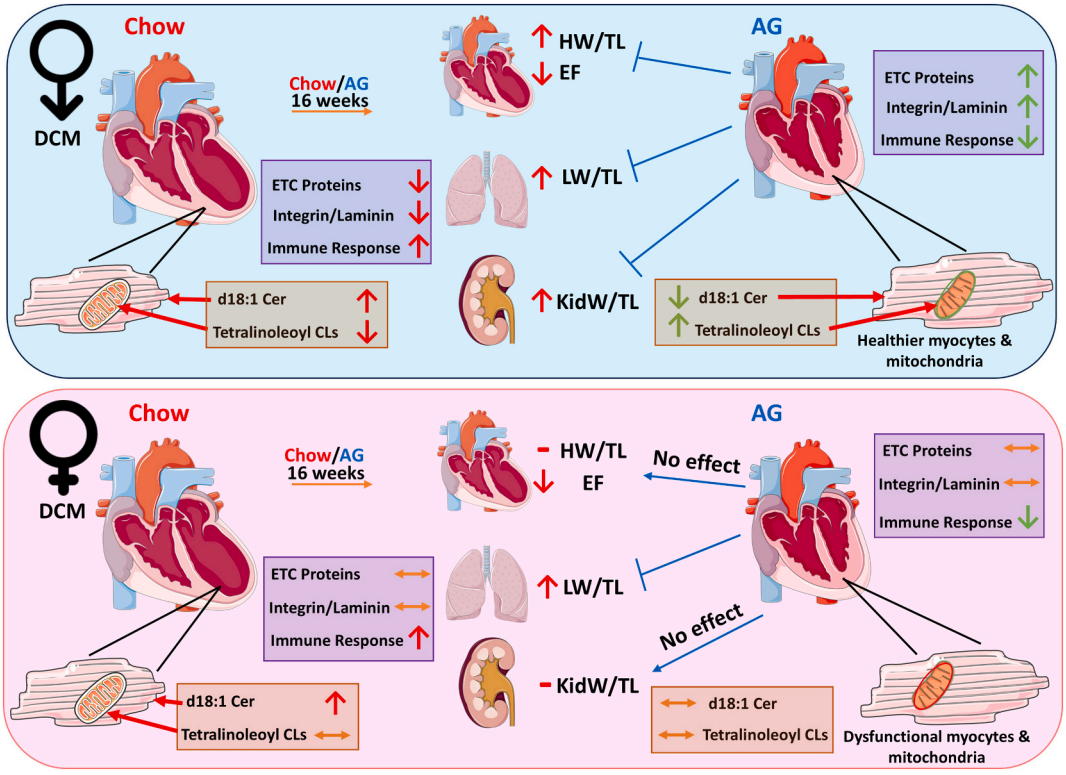

Fig. 6. AG supplementation restored plasmalogens in the DCM hearts but shows greater therapeutic potential in males than females. Top image shows the male DCM heart subjected to chow for 16 weeks. The male DCM chow model is associated with significant increases in HW/TL, LW/TL, and KidW/TL ratios vs. male Ntg chow. EF, a measure of systolic function, is significantly decreased in the DCM model and fell over the 16-week period in male DCM chow mice. Dysfunctional myocytes and mitochondria are associated with significant increases in ceramides and significant decreases in cardiolipins. Furthermore, extracellular matrix proteins and integrin/laminin associated proteins are significantly decreased and immune responses are significantly increased. However, when subjected to the AG diet, this supplementation was able to attenuate HW/TL, LW/TL, and KidW/TL, as well as remodel the cardiac lipidome with a significant decrease in ceramides and a significant increase in cardiolipins. The AG diet was also able to remodel the proteome by significantly increasing extracellular matrix proteins and integrin/laminin associated proteins and significantly decrease immune responses. Therefore, contributing to healthier myocytes and mitochondria. The bottom image shows the female DCM heart subjected to the same conditions. In female DCM chow mice, there was no significant increase in HW/TL or Kid/TL vs. female Ntg chow, and the AG supplement had no effect. LW/TL was increased in female DCM chow mice vs. Ntg, and this was attenuated with the AG diet. EF was lower in female DCM chow mice vs. Ntg, but EF did not fall significantly over the 16-week study. Extracellular matrix proteins and integrin/laminin associated proteins remained unchanged with AG supplementation, however, there was a significant decrease in immune response. LW may be lower with the AG supplement in the male and female DCM model due to a direct impact of plasmalogens on the lungs. In the male DCM model, there could be a further indirect impact due to the AG supplement attenuating cardiac dysfunction. There was no change to the cardiac lipidome in the female DCM mice, therefore contributing to dysfunctional myocytes and mitochondria. Collectively, this would contribute to a greater therapeutic impact in DCM males than DCM females. Abbreviations: AG-Alkylglycerol supplementation, DCM-dilated cardiomyopathy, EF-ejection fraction, HW-heart weight, KidW-kidney weight, LW-lung weight, TL-tibia length.

tetralineoylcardiolipins, was decreased in male chow DCM hearts, and higher in AG supplemented DCM hearts. Loss of tetralineoylcardiolipins in the heart is associated with HF, and conversely, restoration of its levels attenuated mitochondrial dysfunction [40,41]. Collectively, changes to these lipids would suggest that AG supplementation in male DCM mice is associated with reduced inflammation and improved mitochondrial health, thereby contributing to attenuation of cardiac pathology and sustained cardiac function in male DCM mice. These same

changes in Cer and CL lipids did not occur in hearts of female DCM mice.

To gain additional mechanistic insight into how increased plasmalogens in the DCM male heart may confer benefits, proteomic profiling of cardiac tissues was undertaken. AG supplementation in DCM mice was associated with a significant increase or trend for an increase in many key proteins in all five mitochondrial electron transport chain (ETC) complexes compared to chow fed DCM mice (Fig. 7). Notably, expression of these proteins was also significantly decreased in chow fed DCM vs. Ntg hearts. Lipidomic profiling had highlighted the increase in tetralineoylcardiolipins in AG supplemented DCM hearts. The ETC is situated in the inner mitochondria membrane [42], which has a tubular structure with highly curved membrane surfaces that are enriched with CL and PE(P) lipids [43,44]. Notably, both CL and PE(P)s are crucial for the stability and function of the ETC, with loss of PE(P) resulting in decreased expression and activity of the ETC complexes, as well as its disassembly [45]. An overall increase in plasmalogen levels following AG supplementation may therefore contribute to maintaining mitochondrial morphology, specifically the inner mitochondrial membrane which may further lead to maintaining ETC function in generating ATP.

Gene Ontology enrichment analyses in male DCM AG vs. chow hearts further revealed upregulation of proteins involved in extracellular matrix binding (PXDN, TINAGL1, AGRN, DAG1, ADAMTSL5, NID1), integrin mediated signaling (LAMB1, NID1, ITGA5, FN1, RCC2, ITGA1) and laminin-1 complex formation (LAMB1, LAMC1). Differential analysis of the male DCM AG vs. chow proteins also showed that the proteins AGRN, DAG1, ACTN1, LAMA4, Col18a1 and NID1 identified in these enrichment analyses were within the top 10 most significantly upregulated proteins (Supp Table 10). Agrin (AGRN) expression decreases with age in the human heart [46] and is associated with cardiac regeneration [47,48]. α-Dystroglycan (DAG1) is an agrin receptor situated on the plasma membrane, and also serves to attach other ECM proteins like agrin and laminin (LAMB1, LAMC1) to the cytoskeleton. Additionally, α-Dystroglycan is also attached to the dystrophin-glycoprotein complex, which includes dystrophin, sarcospan, the sarcoglycan complex, laminin and syntrophin. The dystrophin-glycoprotein complex forms the crucial connection between the internal cytoskeleton to extracellular laminin, enabling the transmission of mechanical force to the extracellular matrix [19]. Absence or mutations to component proteins within the dystrophin-glycoprotein complex and its associated proteins, such as integrins, have been linked with cardiac pathologies and HF [49]. Further, a recent study that subjected Tg mice lacking plasmalogens in the heart to myocardial infarction implicated plasmalogens providing protection following AG supplementation via a mechanism involving plasma membrane localization of the integrin ITGB3 [50]. In the current study, the integrin proteins and proteins up/downstream of them were significantly upregulated with AG supplementation in the DCM vs. chow DCM hearts, and may contribute to the reduced pathology (Fig. 7).

Agrin is better known for its involvement in neuromuscular function, where it can initiate aggregation of acetylcholine receptors (AChR) via the muscle-specific kinase (MuSK) and low-density lipoprotein receptor-related protein 4 (Lrp4) receptor complex. Plasmalogen deficient mice demonstrated significantly impaired structure and function of the neuromuscular junction, with smaller and fewer clustering of AChR per myotube area vs. wildtype tubes [51]. While Lrp4, MuSK or AchR were not detected within our proteomics screen, studies have shown that the amount and type of plasmalogens present could have a significant effect on neurotransmitter release and vesicular fusion [51–53]. In the context of the DCM heart, this could contribute to the sustained cardiac contractility and function.

Plasmalogens have the capacity to affect multiple signaling pathways because they form a significant part of the cellular membrane, where its presence can affect membrane bilayer thickness, fluidity and lateral

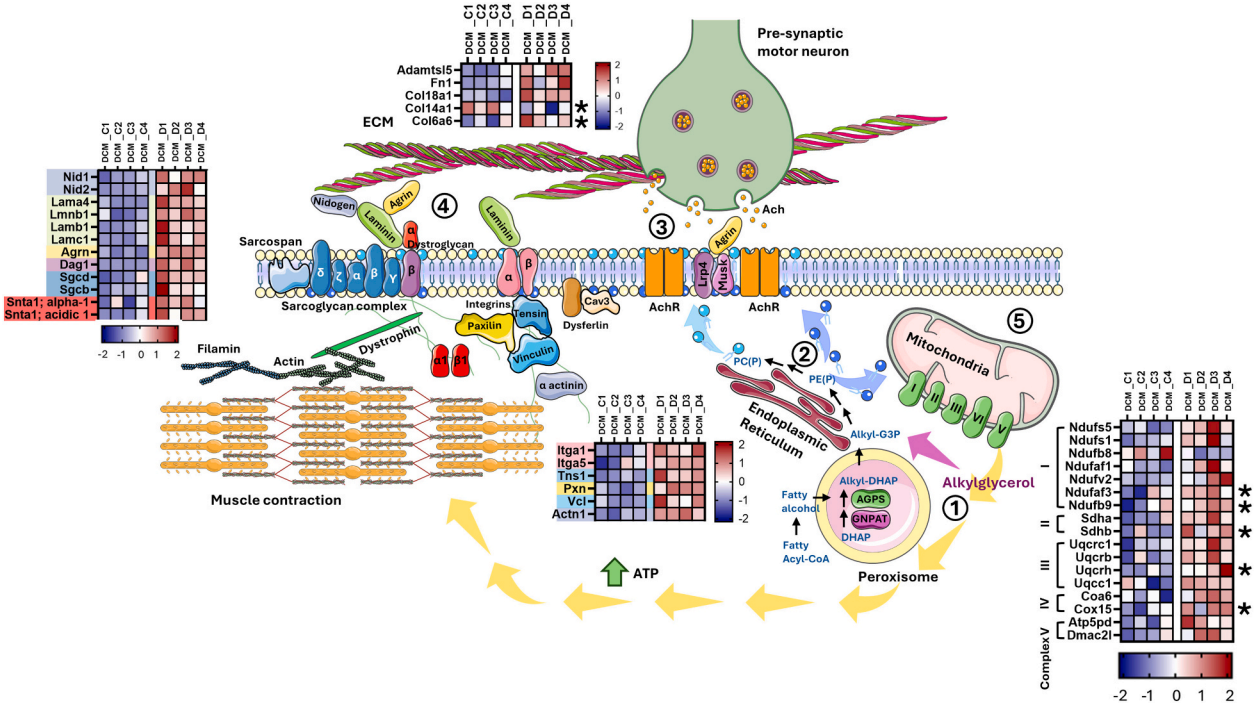

Fig. 7. Potential pathways by which AG supplementation attenuates pathology in the DCM heart. 1. AG supplementation provides metabolic precursors that bypass the rate limiting step of the plasmalogen biosynthesis pathway in the peroxisome. 2. Increased synthesis of plasmalogens [PC(P) and PE(P)] from the endoplasmic reticulum, and its subsequent incorporation into cellular and organelle membranes. 3. Plasmalogen enrichment associated with increased agrin expression that may improve neurotransmitter release between motor neuron and cardiac muscle. 4. Increased plasmalogen levels are further associated with increases in proteins involved in the agrin-dystrophin-glycoprotein and integrin complexes, potentially contributing to positive ECM remodeling and preserving mechanical force transmission to the ECM. 5. Enrichment of plasmalogens in the inner mitochondrial membrane maintains membrane integrity, allowing for sustained electron transport chain functionality for ATP generation to further sustain cardiac muscle contraction. Proteomic results displayed as z-score. All highlighted proteins were statistically significant ($p < 0.05$ vs DCM chow via unpaired *t*-test). Proteins highlighted with * were statistically between $p < 0.1$ and $p > 0.05$.

pressure [54]. Studies have also indicated their propensity to accumulate in lipid raft microdomains and are required for lipid raft stability [55,56]. These changes contribute to modulation of function, recruitment, oligomerization and interaction of plasma membrane and signaling proteins [57–59].

The DCM heart is characterized by increased apoptosis and inflammation, the latter resulting in recruitment of immune cells and activation of the innate and adaptive immune response [3,60]. Enhanced plasmalogen levels following AG supplementation in DCM mice of both sexes resulted in negative enrichment of many Gene Ontology pathways associated with the immune response (Supp Tables 9, 16). While this may usually be associated with a therapeutic benefit, it would appear that this is not the case in the current DCM model given the lack of therapeutic effect in female DCM mice.

There are a number of reasons why the AG diet may have provided more protection in the male DCM model than the female DCM model. Proteomic and lipidomic analyses point to sustained morphology and function in male DCM hearts from AG supplemented mice based on increased mitochondrial ETC protein expression and tetralinoleoylcardiolipin levels which were not observed in females. Additionally, the integrin, dystrophin-glycoprotein complexes and downstream proteins that were significantly increased with AG supplementation in male DCM hearts largely remained unchanged in the female DCM heart following supplementation. These differences could be due to 1) sex specific response to AG supplementation in this DCM model, and/or 2) sex differences in underlying cardiac pathology that are well described in animals and humans. Transcriptomic profiling has shown clear sexual dimorphism in the hearts of the current DCM model, including in response to a therapeutic intervention [6,61–63]. Thus, the mechanisms underlying cardiac pathology in this model will differ based on biological sex, and subsequently, the effects of therapeutic interventions will also differ. It is also noteworthy that in contrast to the male chow DCM mice, in which systolic function fell over the time course of the study, this was not observed in female chow DCM mice. Unexpectedly, systolic function was low in female DCM mice prior to the AG supplement, and function did not deteriorate over time, limiting an ability to observe a change in heart function. Further, the female DCM mice appeared to have less cardiac and renal pathology at endpoint vs. male DCM mice based on an absence of a significant increase in normalized heart weight or kidney weight.

The development of novel therapeutics for individuals with an increased cardiac risk profile using a dietary supplement offers a cost-effective and minimally invasive treatment, ensuring accessibility across diverse socioeconomic domains. Elevating plasmalogen levels was successful and safely achieved in overweight/obese individuals using a shark liver oil supplement, and this was associated with improvement in circulating markers of dyslipidemia and inflammation [16].

5. Conclusion

In summary, to our knowledge, this study describes the first plasmalogen modulating diet to show therapeutic potential for the heart, lungs, and kidneys in a preclinical model of DCM. Here, we show that elevating circulating and cardiac plasmalogens with an optimized AG supplement in DCM mice remodels the cardiac lipidome and proteome, and attenuates pathological features associated with DCM, including cardiac, lung, and kidney enlargement. However, this approach provided greater protection in males than females and highlights the importance of including both sexes in preclinical and clinical research.

CRediT authorship contribution statement

Teleah G. Belkin: Data curation, Formal analysis, Investigation, Methodology, Validation, Visualization, Writing – original draft, Writing – review & editing. **Emma I. Masterman:** Formal analysis, Investigation. **Gunes S. Yildiz:** Formal analysis, Investigation. **Helen Kiriazis:** Investigation, Validation. **Natalie A. Mellett:** Data curation, Validation. **Jonathon Cross:** Data curation, Formal analysis, Investigation, Visualization. **Kyah Grigolon:** Formal analysis, Validation. **Akshima Dogra:** Formal analysis, Validation. **Daniel Donner:** Resources, Validation. **Roger Chooi:** Validation. **Amy Liang:** Data curation, Software. **Andrew R. Kompa:** Resources, Validation. **Junichi Sadoshima:** Resources. **Amanda J. Edgley:** Resources, Supervision, Validation. **David W. Greening:** Data curation, Formal analysis, Resources, Validation. **Peter J. Meikle:** Conceptualization, Methodology, Resources. **Yow Keat Tham:** Conceptualization, Data curation, Formal analysis, Funding acquisition, Investigation, Project administration, Supervision, Validation, Visualization, Writing – review & editing. **Julie R. McMullen:** Conceptualization, Funding acquisition, Investigation, Project administration, Resources, Supervision, Validation, Writing – review & editing.

Declaration of Generative AI and AI-assisted technologies in the writing process

The authors did not use generative AI or AI-assisted technologies in the development of this manuscript.

Sources of funding

This work was supported by grants from the National Health and Medical Research Council (Project grant: 1045585 to J.R.M), the National Heart Foundation of Australia (Vanguard grant: 105563 to Y.K.T and J.R.M) and in part by the Victorian Government's Operational Infrastructure Support Program. T.G.B is supported by an Australian Government Research Training Program scholarship. J.R.M was supported by a National Health and Medical Research Council Senior Research Fellowship [grant number 1078985] and Baker Fellowship (The Baker Foundation, Australia).

Declaration of competing interest

The authors declare the following financial interests/personal relationships which may be considered as potential competing interests: Julie R McMullen reports financial support was provided by NHMRC. Yow Keat Tham reports financial support was provided by National Heart Foundation of Australia. Julie R McMullen reports financial support was provided by National Heart Foundation of Australia. Julie R McMullen has patent #15768.6018 pending to Baker Heart and Diabetes Institute. Yow Keat Tham has patent #15768.6018 pending to Baker Heart and Diabetes Institute. Peter Meikle has patent #15768.6018 pending to Baker Heart and Diabetes Institute. Julie McMullen is an Associate Editor of JMCC-PLUS. This paper was originally submitted to JMCC (Julie McMullen does not serve on the editorial board of JMCC) If there are other authors, they declare that they have no known competing financial interests or personal relationships that could have appeared to influence the work reported in this paper.

Appendix A. Supplementary data

Supplementary data to this article can be found online at https://doi.org/10.1016/j.jmccpl.2024.100273.

Data availability

Mass spectrometry lipidomic data is available at the NIH Common Fund's National Metabolomics Data Repository (NMDR) website, the Metabolomics Workbench (https://dev.metabolomicsworkbench.org:22222/data/DRCCMetadata.php?Mode=Study&StudyID=ST003472&Access=VsmW5225) [64]. Mass spectrometry proteomics data is deposited to the ProteomeXchange

Consortium via the MASSive partner repository and available via MASSive with identifier (*MSV000095560-https://massive.ucsd.edu/ProteoSAFe/dataset.jsp?task=be73406454924134a62d5bf36a883672*).

References

[1] Panganamala RV, Horrocks LA, Geer JC, Cornwell DG. Positions of double bonds in the monounsaturated alk-1-enyl groups from the plasmalogens of human heart and brain. Chem Phys Lipids 1971;6:97–102. https://doi.org/10.1016/0009-3084(71)90031-4.

[2] Heymans HS, Schutgens RB, Tan R, van den Bosch H, Borst P. Severe plasmalogen deficiency in tissues of infants without peroxisomes (Zellweger syndrome). Nature 1983;306:69–70.

[3] Yamamoto S, Yang G, Zablocki D, Liu J, Hong C, Kim SJ, et al. Activation of Mst1 causes dilated cardiomyopathy by stimulating apoptosis without compensatory ventricular myocyte hypertrophy. J Clin Invest 2003;111:1463–74. https://doi.org/10.1172/JCI17459.

[4] Maejima Y, Kyoi S, Zhai P, Liu T, Li H, Ivessa A, et al. Mst1 inhibits autophagy by promoting the interaction between Beclin1 and Bcl-2. Nat Med 2013;19:1478–88. https://doi.org/10.1038/nm.3322.

[5] Odashima M, Usui S, Takagi H, Hong C, Liu J, Yokota M, et al. Inhibition of endogenous Mst1 prevents apoptosis and cardiac dysfunction without affecting cardiac hypertrophy after myocardial infarction. Circ Res 2007;100:1344–52. https://doi.org/10.1161/01.RES.0000265846.23485.7a.

[6] Tham YK, Bernardo BC, Claridge B, Yildiz GS, Woon LM-L, Bond S, et al. Estrogen receptor alpha deficiency in cardiomyocytes reprograms the heart-derived extracellular vesicle proteome and induces obesity in female mice. Nat Cardiovasc Res 2023;2:268–89. https://doi.org/10.1038/s44161-023-00223-z.

[7] Claridge B, Rai A, Fang H, Matsumoto A, Luo J, McMullen JR, et al. Proteome characterisation of extracellular vesicles isolated from heart. Proteomics 2021;21:e2100026. https://doi.org/10.1002/pmic.202100026.

[8] Yew MJ, Heywood SE, Ng J, West OM, Pal M, Kueh A, et al. ACAD10 is not required for metformin's metabolic actions or for maintenance of whole-body metabolism in C57BL/6J mice. Diabetes Obes Metab 2024;26:1731–45. https://doi.org/10.1111/dom.15484.

[9] Tham YK, Huynh K, Mellett NA, Henstridge DC, Kiriazis H, Ooi JYY, et al. Distinct lipidomic profiles in models of physiological and pathological cardiac remodeling, and potential therapeutic strategies. Biochim Biophys Acta Mol Cell Biol Lipids 2018;1863:219–34. https://doi.org/10.1016/j.bbalip.2017.12.003.

[10] Pauschinger M, Knopf D, Petschauer S, Doerner A, Poller W, Schwimmbeck PL, et al. Dilated cardiomyopathy is associated with significant changes in collagen type I/III ratio. Circulation 1999;99:2750–6. https://doi.org/10.1161/01.cir.99.21.2750.

[11] Zhang M, Wang X, Chen W, Liu W, Xin J, Yang D, et al. Integrated bioinformatics analysis for identifying key genes and pathways in female and male patients with dilated cardiomyopathy. Sci Rep 2023;13:8977. https://doi.org/10.1038/s41598-023-36117-0.

[12] Choi RH, Tatum SM, Symons JD, Summers SA, Holland WL. Ceramides and other sphingolipids as drivers of cardiovascular disease. Nat Rev Cardiol 2021. https://doi.org/10.1038/s41569-021-00536-1.

[13] Salatzki J, Foryst-Ludwig A, Bentele K, Blumrich A, Smeir E, Ban Z, et al. Adipose tissue ATGL modifies the cardiac lipidome in pressure-overload-induced left ventricular failure. PLoS Genet 2018;14:e1007171. https://doi.org/10.1371/journal.pgen.1007171.

[14] Wu W, Ziemann M, Huynh K, She G, Pang ZD, Zhang Y, et al. Activation of Hippo signaling pathway mediates mitochondria dysfunction and dilated cardiomyopathy in mice. Theranostics 2021;11:8993–9008. https://doi.org/10.7150/thno.62302.

[15] Paul S, Rasmiena AA, Huynh K, Smith AAT, Mellett NA, Jandeleit-Dahm K, et al. Oral supplementation of an alkylglycerol mix comprising different alkyl chains effectively modulates multiple endogenous plasmalogen species in mice. Metabolites 2021:11. https://doi.org/10.3390/metabo11050299.

[16] Paul S, Smith AAT, Culham K, Gunawan KA, Weir JM, Cinel MA, et al. Shark liver oil supplementation enriches endogenous plasmalogens and reduces markers of dyslipidemia and inflammation. J Lipid Res 2021;62:100092. https://doi.org/10.1016/j.jlr.2021.100092.

[17] Murray IR, Gonzalez ZN, Baily J, Dobie R, Wallace RJ, Mackinnon AC, et al. αv integrins on mesenchymal cells regulate skeletal and cardiac muscle fibrosis. Nat Commun 2017;8:1118. https://doi.org/10.1038/s41467-017-01097-z.

[18] Del Re DP, Matsuda T, Zhai P, Maejima Y, Jain MR, Liu T, et al. Mst1 promotes cardiac myocyte apoptosis through phosphorylation and inhibition of Bcl-xL. Mol Cell 2014;54:639–50. https://doi.org/10.1016/j.molcel.2014.04.007.

[19] Valera IC, Wacker AL, Hwang HS, Holmes C, Laitano O, Landstrom AP, et al. Essential roles of the dystrophin-glycoprotein complex in different cardiac pathologies. Adv Med Sci 2021;66:52–71. https://doi.org/10.1016/j.advms.2020.12.004.

[20] Zbinden A, Layland SL, Urbanczyk M, Carvajal Berrio DA, Marzi J, Zauner M, et al. Nidogen-1 mitigates ischemia and promotes tissue survival and regeneration. Adv Sci (Weinh) 2021;8:2002500. https://doi.org/10.1002/advs.202002500.

[21] Li J, Salvador AM, Li G, Valkov N, Ziegler O, Yeri A, et al. Mir-30d regulates cardiac remodeling by intracellular and paracrine signaling. Circ Res 2021;128:e1–23. https://doi.org/10.1161/circresaha.120.317244.

[22] Gu J, Chen L, Sun R, Wang JL, Wang J, Lin Y, et al. Plasmalogens eliminate aging-associated synaptic defects and microglia-mediated neuroinflammation in mice. Front Mol Biosci 2022;9:815320. https://doi.org/10.3389/fmolb.2022.815320.

[23] Braverman N, Zhang R, Chen L, Nimmo G, Scheper S, Tran T, et al. A Pex7 hypomorphic mouse model for plasmalogen deficiency affecting the lens and skeleton. Mol Genet Metab 2010;99:408–16. https://doi.org/10.1016/j.ymgme.2009.12.005.

[24] Rasmiena AA, Barlow CK, Stefanovic N, Huynh K, Tan R, Sharma A, et al. Corrigendum to "Plasmalogen modulation attenuates atherosclerosis in ApoE- and ApoE/GPx1-deficient mice" [Atherosclerosis 243/2 (2015) 598-608]. Atherosclerosis 2016;254:314–5. https://doi.org/10.1016/j.atherosclerosis.2016.01.046.

[25] Todt H, Dorninger F, Rothauer PJ, Fischer CM, Schranz M, Bruegger B, et al. Oral batyl alcohol supplementation rescues decreased cardiac conduction in ether phospholipid-deficient mice. J Inherit Metab Dis 2020;43:1046–55. https://doi.org/10.1002/jimd.12264.

[26] Honsho M, Asaoku S, Fujiki Y. Posttranslational regulation of fatty acyl-CoA reductase 1, Far1, controls ether glycerophospholipid synthesis. J Biol Chem 2010;285:8537–42. https://doi.org/10.1074/jbc.M109.083311.

[27] Giam B, Kuruppu S, Chu PY, Smith AI, Marques FZ, Fiedler A, et al. N-acetylcysteine attenuates the development of renal fibrosis in transgenic mice with dilated cardiomyopathy. Sci Rep 2017;7:17718. https://doi.org/10.1038/s41598-017-17927-5.

[28] Li H, Feng J, Zhang Y, Feng J, Wang Q, Zhao S, et al. Mst1 deletion attenuates renal ischaemia-reperfusion injury: the role of microtubule cytoskeleton dynamics, mitochondrial fission and the GSK3β-p53 signalling pathway. Redox Biol 2019;20:261–74. https://doi.org/10.1016/j.redox.2018.10.012.

[29] Yang T, Heng C, Zhou Y, Hu Y, Chen S, Wang H, et al. Targeting mammalian serine/threonine-protein kinase 4 through yes-associated protein/TEA domain transcription factor-mediated epithelial-mesenchymal transition ameliorates diabetic nephropathy orchestrated renal fibrosis. Metabolism 2020;108:154258. https://doi.org/10.1016/j.metabol.2020.154258.

[30] Liang J, Zhu R, Yang Y, Li R, Hong C, Luo C. A predictive model for dilated cardiomyopathy with pulmonary hypertension. ESC Heart Fail 2021;8:4255–64. https://doi.org/10.1002/ehf2.13535.

[31] Karnati S, Baumgart-Vogt E. Peroxisomes in airway epithelia and future prospects of these organelles for pulmonary cell biology. Histochem Cell Biol 2009;131:447–54. https://doi.org/10.1007/s00418-009-0566-4.

[32] Berry KA, Hankin JA, Barkley RM, Spraggins JM, Caprioli RM, Murphy RC. MALDI imaging of lipid biochemistry in tissues by mass spectrometry. Chem Rev 2011;111:6491–512. https://doi.org/10.1021/cr200280p.

[33] Trentin-Sonoda M, da Silva RC, Kmit FV, Abrahão MV, Monnerat Cahli G, Brasil GV, et al. Knockout of toll-like receptors 2 and 4 prevents renal ischemia-reperfusion-induced cardiac hypertrophy in mice. PLoS One 2015;10:e0139350. https://doi.org/10.1371/journal.pone.0139350.

[34] Wang DD, Toledo E, Hruby A, Rosner BA, Willett WC, Sun Q, et al. Plasma ceramides, Mediterranean diet, and incident cardiovascular disease in the PREDIMED trial (Prevención con Dieta Mediterránea). Circulation 2017;135:2028–40. https://doi.org/10.1161/circulationaha.116.024261.

[35] Ji R, Akashi H, Drosatos K, Liao X, Jiang H, Kennel PJ, et al. Increased de novo ceramide synthesis and accumulation in failing myocardium. JCI Insight 2017;2:e82922. https://doi.org/10.1172/jci.insight.82922.

[36] Ji R, Akashi H, Drosatos K, Liao X, Jiang H, Kennel PJ, et al. Increased de novo ceramide synthesis and accumulation in failing myocardium. JCI Insight 2017:2. https://doi.org/10.1172/jci.insight.96203.

[37] Bielawska AE, Shapiro JP, Jiang L, Melkonyan HS, Piot C, Wolfe CL, et al. Ceramide is involved in triggering of cardiomyocyte apoptosis induced by ischemia and reperfusion. Am J Pathol 1997;151:1257–63.

[38] Law BA, Liao X, Moore KS, Southard A, Roddy P, Ji R, et al. Lipotoxic very-long-chain ceramides cause mitochondrial dysfunction, oxidative stress, and cell death in cardiomyocytes. FASEB J 2018;32:1403–16. https://doi.org/10.1096/fj.201700300R.

[39] Schlame M, Ren M, Xu Y, Greenberg ML, Haller I. Molecular symmetry in mitochondrial cardiolipins. Chem Phys Lipids 2005;138:38–49. https://doi.org/10.1016/j.chemphyslip.2005.08.002.

[40] Mulligan CM, Sparagna GC, Le CH, De Mooy AB, Routh MA, Holmes MG, et al. Dietary linoleate preserves cardiolipin and attenuates mitochondrial dysfunction in the failing rat heart. Cardiovasc Res 2012;94:460–8. https://doi.org/10.1093/cvr/cvs118.

[41] Sparagna GC, Chicco AJ, Murphy RC, Bristow MR, Johnson CA, Rees ML, et al. Loss of cardiac tetralinoleoyl cardiolipin in human and experimental heart failure. J Lipid Res 2007;48:1559–70. https://doi.org/10.1194/jlr.M600551-JLR200.

[42] Nolfi-Donegan D, Braganza A, Shiva S. Mitochondrial electron transport chain: oxidative phosphorylation, oxidant production, and methods of measurement. Redox Biol 2020;37:101674. https://doi.org/10.1016/j.redox.2020.101674.

[43] Ikon N, Ryan RO. Cardiolipin and mitochondrial cristae organization. Biochim Biophys Acta Biomembr 2017;1859:1156–63. https://doi.org/10.1016/j.bbamem.2017.03.013.

[44] Kimura T, Kimura AK, Ren M, Monteiro V, Xu Y, Berno B, et al. Plasmalogen loss caused by remodeling deficiency in mitochondria. Life Sci Alliance 2019:2. https://doi.org/10.26508/lsa.201900348.

[45] Vance JE, Tasseva G. Formation and function of phosphatidylserine and phosphatidylethanolamine in mammalian cells. Biochim Biophys Acta 2013;1831:543–54. https://doi.org/10.1016/j.bbalip.2012.08.016.

[46] Skeffington KL, Jones FP, Suleiman MS, Caputo M, Brancaccio A, Bigotti MG. Determination of agrin and related proteins levels as a function of age in human

hearts. Front Cardiovasc Med 2022;9:813904. https://doi.org/10.3389/fcvm.2022.813904.
[47] Bassat E, Mutlak YE, Genzelinakh A, Shadrin IY, Baruch Umansky K, Yifa O, et al. The extracellular matrix protein agrin promotes heart regeneration in mice. Nature 2017;547:179–84. https://doi.org/10.1038/nature22978.
[48] Baehr A, Umansky KB, Bassat E, Jurisch V, Klett K, Bozoglu T, et al. Agrin promotes coordinated therapeutic processes leading to improved cardiac repair in pigs. Circulation 2020;142:868–81. https://doi.org/10.1161/CIRCULATIONAHA.119.045116.
[49] Wilson DGS, Tinker A, Iskratsch T. The role of the dystrophin glycoprotein complex in muscle cell mechanotransduction. Commun Biol 2022;5:1022. https://doi.org/10.1038/s42003-022-03980-y.
[50] Sun JT, Wang ZM, Zhou LH, Yang TT, Zhao D, Bao YL, et al. PEX3 promotes regenerative repair after myocardial injury in mice through facilitating plasma membrane localization of ITGB3. Commun Biol 2024;7:795. https://doi.org/10.1038/s42003-024-06483-0.
[51] Dorninger F, Herbst R, Kravic B, Camurdanoglu BZ, Macinkovic I, Zeitler G, et al. Reduced muscle strength in ether lipid-deficient mice is accompanied by altered development and function of the neuromuscular junction. J Neurochem 2017;143:569–83. https://doi.org/10.1111/jnc.14082.
[52] Braverman NE, Moser AB. Functions of plasmalogen lipids in health and disease. Biochim Biophys Acta 2012;1822:1442–52. https://doi.org/10.1016/j.bbadis.2012.05.008.
[53] Breckenridge WC, Morgan IG, Zanetta JP, Vincendon G. Adult rat brain synaptic vesicles. II. Lipid composition. Biochim Biophys Acta 1973;320:681–6. https://doi.org/10.1016/0304-4165(73)90148-7.
[54] Koivuniemi A. The biophysical properties of plasmalogens originating from their unique molecular architecture. FEBS Lett 2017;591:2700–13. https://doi.org/10.1002/1873-3468.12754.
[55] Pike LJ, Han X, Chung KN, Gross RW. Lipid rafts are enriched in arachidonic acid and plasmenylethanolamine and their composition is independent of caveolin-1 expression: a quantitative electrospray ionization/mass spectrometric analysis. Biochemistry 2002;41:2075–88. https://doi.org/10.1021/bi0156557.
[56] Rog T, Koivuniemi A. The biophysical properties of ethanolamine plasmalogens revealed by atomistic molecular dynamics simulations. Biochim Biophys Acta 2016;1858:97–103. https://doi.org/10.1016/j.bbamem.2015.10.023.
[57] Sezgin E, Levental I, Mayor S, Eggeling C. The mystery of membrane organization: composition, regulation and roles of lipid rafts. Nat Rev Mol Cell Biol 2017;18:361–74. https://doi.org/10.1038/nrm.2017.16.
[58] Simons K, Sampaio JL. Membrane organization and lipid rafts. Cold Spring Harb Perspect Biol 2011;3:a004697. https://doi.org/10.1101/cshperspect.a004697.
[59] Koivuniemi A, Vattulainen I. Modeling of lipid membranes and lipoproteins. Springer; 2014.
[60] Tian C, Hu G, Gao L, Hackfort BT, Zucker IH. Extracellular vesicular MicroRNA-27a* contributes to cardiac hypertrophy in chronic heart failure. J Mol Cell Cardiol 2020. https://doi.org/10.1016/j.yjmcc.2020.04.032.
[61] Bernardo BC, Ooi JY, Matsumoto A, Tham YK, Singla S, Kiriazis H, et al. Sex differences in response to miRNA-34a therapy in mouse models of cardiac disease: identification of sex-, disease- and treatment-regulated miRNAs. J Physiol 2016;594:5959–74. https://doi.org/10.1113/JP272512.
[62] Lam CSP, Arnott C, Beale AL, Chandramouli C, Hilfiker-Kleiner D, Kaye DM, et al. Sex differences in heart failure. Eur Heart J 2019;40:3859–3868c. https://doi.org/10.1093/eurheartj/ehz835.
[63] Reue K, Wiese CB. Illuminating the mechanisms underlying sex differences in cardiovascular disease. Circ Res 2022;130:1747–62. https://doi.org/10.1161/CIRCRESAHA.122.320259.
[64] Sud M, Fahy E, Cotter D, Azam K, Vadivelu I, Burant C, et al. Metabolomics Workbench: an international repository for metabolomics data and metadata, metabolite standards, protocols, tutorials and training, and analysis tools. Nucleic Acids Res 2016;44:D463–70. https://doi.org/10.1093/nar/gkv1042.
[65] Fang H, Greening DW. An Optimized Data-Independent Acquisition Strategy for Comprehensive Analysis of Human Plasma Proteome. In: Greening DW, Simpson RJ, editors. Serum/Plasma Proteomics. Methods in Molecular Biology. 2628. New York, NY: Humana; 2023.